Self-assembly of organometallic clusters onto the surface of gold

Ilse Y. Guzman-Jimenez[a], K.H. Whitmire[a],*, Kayo Umezama-Vizzini[b], Ramon Colorado Jr[b],
Junghwan Do[b], Allan Jacobson[b], T. Randall Lee[b], Seunghun Hong[c], Chad A. Mirkin[c]

[a]*Department of Chemistry, Rice University, P.O. Box 1892, Houston, TX 77251, USA*
[b]*Department of Chemistry, University of Houston, Houston, TX 77204, USA*
[c]*Department of Chemistry, Northwestern University, Evanston, IL 60208, USA*

Abstract

We report the preparation and characterization of thin films generated via the solution-phase self-assembly of organometallic chalcogen-containing cluster compounds onto the surface of gold. The following anionic complexes were used as thin film precursors: $[Fe_3(CO)_9E]^{2-}$ and $[HFe_3(CO)_9E]^-$, where E = S, Se, and Te. The films were prepared by adsorption from organic solvents (i.e. methanol, acetonitrile, acetone, and dichloromethane) onto evaporated gold and were characterized by ellipsometry, polarization-modulation infrared reflection-absorption spectroscopy (PM-IRRAS), X-ray diffraction (XRD), atomic force microscopy (AFM), quartz crystal microbalance (QCM) and X-ray photoelectron spectroscopy (XPS). The data demonstrate that the clusters strongly attach to gold and that the films most likely exist as bilayers rather than monolayers. © 2001 Elsevier Science B.V. All rights reserved.

Keywords: Organometallic; Clusters; Self-assembly

1. Introduction

Self-assembled monolayers (SAMs) are most commonly generated by the adsorption of alkanethiols or dialkyl disulfides onto the surface of gold.[1] This technique provides a convenient route to thin films that are highly ordered, well defined and moderately stable [2,3], leading to applications in the field of chemical sensing and optical devices [4]. The two primary factors responsible for SAM formation are: (1) the covalent bond formed between sulfur and gold; and (2) the van der Waals' interactions between the alkane chains [5,6]. Control over both the micro- and macroscopic interfacial properties can be achieved by appropriate choice of the organosulfur moiety. While organic films containing selenol, diselenide and telluride as anchor groups instead of the typical sulfur-containing moieties have been reported to form ordered phases, the structures are different from those of alkanethiol- and dialkyl disulfide-based SAMs [7,8], indicating a chalcogen-dependent assembly process [9,10]. The self-assembly of inorganic adsorbates has received relatively little attention due to the fact that few purely inorganic molecules are adaptable to standard SAM methods [11,12]. Transition-metal cluster compounds containing chalcogenide sites, however, offer the unique opportunity of exploring the self-assembly of inorganic molecules using traditional chalcogens as anchors. In the present report, we describe the interaction of six iron cluster complexes, $[Fe_3(CO)_9E]^{2-}$ and $[HFe_3(CO)_9E]^-$ (E = S, Se, and Te) with the surface of gold.

2. Experimental

2.1. Materials and general methods

All manipulations were performed using standard techniques on a Schlenk line or in a Vacuum Atmos-

---

* Corresponding author. Tel.: +1-713-348-5650; fax: +1-713-348-5652.

E-mail address: whitmir@rice.edu (K.H. Whitmire).

pheres inert atmosphere box [13]. Solvents were distilled from the appropriate drying agent under nitrogen prior to use: methanol, acetonitrile, hexane, acetone, ethanol and dichloromethane (CaH_2); THF and diethyl ether (Na/Ph_2CO). The complexes $[PPN]_2[Fe_3(CO)_9S]$ [14], $[PPN]_2[Fe_3(CO)_9Se]$ [15], $[PPN]_2[Fe_3(CO)_9Te]$ [15], $[Et_4N]_2[Fe_3(CO)_9S]$, $[Et_4N]_2[Fe_3(CO)_9Se]$ and $[Et_4N]_2[Fe_3(CO)_9Te]$ were prepared according to the literature methods indicated for the bis(triphenylphosphine)iminium (PPN^+) salt, but using tetraethylammonium (Et_4N^+) instead. $[Et_4N][HFe_3(CO)_9S]$ and $[Et_4N][HFe_3(CO)_9Se]$ were prepared as the analogue $[Et_4N][HFe_3(CO)_9Te]$ [16].

2.2. Preparation of self-assembled films

The gold substrates were generated by vacuum evaporation of ~ 2000 Å of gold onto silicon (100) wafers that were precoated with ~ 100 Å of chromium (to promote adhesion of gold). Self-assembled films were prepared by immersing small pieces of the freshly prepared gold-coated wafers in solutions containing the appropriate clusters (0.5 mM) for 24 h, unless otherwise indicated. The various solvents employed in these experiments included methanol, acetonitrile, acetone and dicholoromethane. After removal from solution, the slides were rinsed thoroughly with the same solvent used in the solutions; the solvent was removed by placing the slides under vacuum in the antechamber of the inert-atmosphere box for 5 min. Samples prepared on Au(111)/mica were used for atomic force microscopy (AFM) measurements. The Au(111)/mica substrates were prepared with a Veeco model VE400 thermal evaporator operating at a base pressure of 10^{-6} torr and equipped with an Inficon XTC 6 MHz quartz crystal microbalance to control the rate of deposition and measure the mass thickness of the film. The Au(111)/mica films were epitaxially grown onto freshly cleaved mica by resistively heating Au wire (99.95%, Aldrich) in a tungsten boat source (R.D. Mathis, Long Beach, CA) at a deposition rate of 0.03 nm s^{-1} and a substrate temperature of 240°C.

2.3. Characterization of SAMs

The thickness of the films was measured with a Rudolf Research Auto EL III ellipsometer, which employs a He–Ne laser beam of 632 nm at an angle of incidence of 70°. A refractive index value of $n = 1.282$ was used in calculations of the ellipsometric thickness for all films. The infrared studies employed polarization-modulation infrared reflection absorption spectroscopy (PM-IRRAS), the spectra were collected over 256 scans at a spectral resolution of 4 cm^{-1}, using a Nicolet MAGNA-IR 860 Fourier-transform spectrometer equipped with a liquid nitrogen-cooled mercury–cadmi-

um–telluride (MCT) detector and a Hinds Instruments PEM-90 photoelastic modulator (37 kHz). The light was reflected from the samples at an angle of 80°. The X-ray photoelectron spectroscopy (XPS) data of freshly prepared samples were obtained using a PHI 5750 X-ray photoelectron spectrometer equipped with a monochromatic AlK_α X-ray source ($h\nu = 1486.7$ eV). All XPS data were obtained at room temperature and a base pressure of 2×10^{-9} torr using a pass energy of 23.5 eV, a photoelectron take-off angle of 45° from the surface, and analyzer spot diameter of 1.1 mm. Intensities were calculated with standard curve-fitting software using a Shirley background subtraction and Gaussian–Lorentzian curves. Data from XRD experiments were collected using a Scintag XDS 2000 automated powder X-ray diffractometer, $\lambda = 1.54178$ Å, θ–θ geometry. Atomic force microscopy (AFM) measurements were obtained with Thermomicroscopes model CP AFM with a combined AFM/LFM head. Sharpened silicon-nitride cantilevers (model MLCT-AUNM) were purchased from Thermomicroscopes. On top of these silicon nitride tips, a 300-nm-long rigid carbon rod with ~ 5-nm diameter was added by the electron-beam deposition method (fabricated by NanoTOOLS GmbH, Type 1S). These tips with extremely sharp ends minimize the tip convolution effect and provide more precise dimensional information on the molecular layers. When an atomic force microscope is operated in air, water condenses between the tip and surface and the capillary force associated with it significantly impedes the operation of the AFM, especially when run in lateral force mode. AFM tips were coated with dodecylamine molecules to minimize this capillary effect [17]. Quartz crystal microbalance (QCM) measurements were performed on a Maxtek PM710 microbalance. A 5-MHz AT cut quartz crystal with vapor-deposited gold electrodes obtained from Maxtek was used with the microbalance, having a resolution of the order of 0.03 Hz, which translates to a mass resolution of 0.7 ng cm^{-2}. Frequency changes were converted to mass loading using the Sauerbrey [18] formula. All measurements were performed in situ using standard inert-atmosphere techniques. Glassware and quartz crystals were cleaned with H_2O_2 (30%)/ H_2SO_4 (1:3) for 5 min and rinsed with deionized water. Glassware was subsequently rinsed with acetone and dried in an oven; quartz crystals were rinsed with ethanol and dried under a stream of high-purity N_2.

3. Results and discussion

As shown in Fig. 1, the cluster compounds chosen for study contain a tetrahedral structure composed of a triangular Fe_3 framework capped by an E atom (E = S, Se, and Te). The clusters $[Fe_3(CO)_9E]^{2-}$ undergo protonation to yield $[HFe_3(CO)_9E]^-$, in which the hydrogen atom adopts a bridging configuration. The dianion
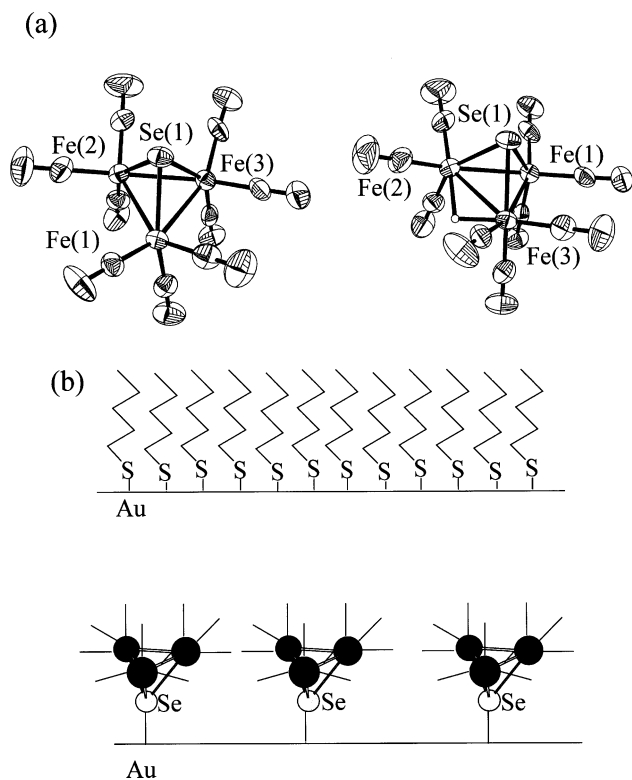
(a)

(b)

Fig. 1. (a) ORTEP diagram of $[Fe_3(CO)_9E]^{2-}$ and $[HFe_3(CO)_9E]^{-}$ (E=Se). (b) Graphic representation of the self-assembled film formed upon adsorption of $[Fe_3(CO)_9E]^{2-}$ onto the surface of gold.

$[Fe_3(CO)_9E]^{2-}$ is quantitatively monoprotonated in methanol; consequently, in this solvent, the primary species present is the $[HFe_3(CO)_9E]^{-}$ anion [16,19].

Our investigation of the self-assembly of these organometallic clusters began with an examination of films prepared in a series of different solvents and using either bis(triphenylphosphine)iminium (PPN^{+}) or tetraethylammonium (Et$_4$N^{+}) as counterions. After immersion for 24 h, followed by rinsing and drying, we characterized the samples using a variety of analytical techniques. In an initial set of studies, films formed from $[HFe_3(CO)_9E]^{-}$ (E=S, Se, and Te) and $[Fe_3(CO)_9E]^{-}$ (E=S, and Se) were analyzed by PM-IRRAS in the ν(C–O) region of ∼1750–2250 cm^{-1}. We were able to observe carbonyl bands only when the Et$_4$N^{+} salt was used as the counterion (see Fig. 2). This result not only indicates that the cation plays a significant role in the assembly of the cluster, but is also consistent with a model for adsorption in which smaller cations allow for better packing between the clusters. For the films formed from the Et$_4$N^{+} salts of $[Fe_3(CO)_9E]^{2-}$ and $[HFe_3(CO)_9E]^{-}$, characteristic ν(C–O) bands were observed (Fig. 2), but their position was shifted by approximately 30–60 cm^{-1} compared to simple transmission IR spectra of $[Fe_3(CO)_9E]^{2-}$ and $[HFe_3(CO)_9E]^{-}$ in solution [14–16,19]. The frequency

shifts are consistent with the removal of electron density from the clusters, as would be expected upon binding to an electropositive center.

The observation of characteristic ν(C–O) patterns for adsorbed $[Fe_3(CO)_9E]^{2-}$ and $[HFe_3(CO)_9E]^{-}$ species suggests that the clusters remain intact, while strongly interacting with the surface of gold. We found that starting with either $[Et_4N][HFe_3(CO)_9Se]$ or $[Et_4N]_2[Fe_3(CO)_9Se]^{2-}$ in methanol gave essentially identical results, owing to the facile protonation of the dianion in the protic solvent. Furthermore, given that $[HFe_3(CO)_9Se]^{-}$ in methanol afforded consistently reproducible films by PM-IRRAS and ellipsometry (vide infra), we chose to focus our remaining analyses using this adsorbate and solvent.

Analysis of the $[HFe_3(CO)_9Se]^{-}$ films by XRD showed the presence of a single, weak diffraction peak at $2\theta = 2.1°$ corresponding to a d-spacing of ∼41 Å (data not shown). No higher-order reflections were observed, indicating that the films have limited long-range order. The observation of a single diffraction peak suggests a bilayer, in which each layer has a thickness of $41/n$ Å, where n is an integer. The data are, however, insufficient to distinguish among the possible values of n. In addition, other structures that differ, for example, in cluster orientation, cannot be ruled out by these data.

Since the refractive index of the iron cluster is unknown, we decided to extrapolate this value by varying the refractive index input in a fixed-angle ellipsometer. A value of $n = 1.282$ yielded a thickness value comparable with the data obtained from the XRD experiments, where it appeared that the thickness was ∼41 Å. We measured the ellipsometric thickness for films prepared at various adsorbate concentrations and times of deposition (see Fig. 3a,b). While the *absolute*
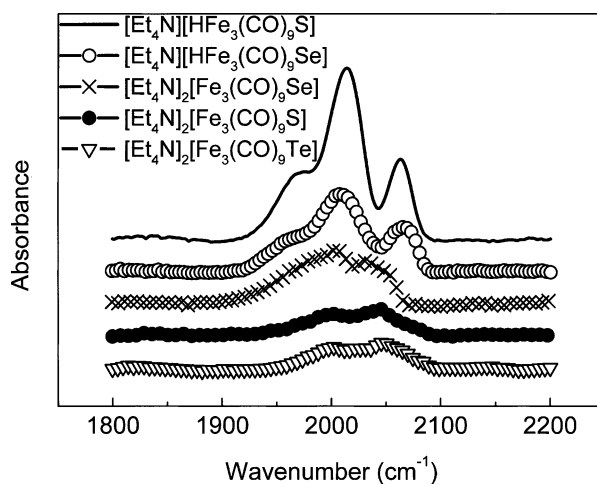

Fig. 2. PM-IRRAS of film formed from the adsorption of $[HFe_3(CO)_9E]^{-}$ (E=S, Se, and Te) and $[Fe_3(CO)_9E]^{-}$ (E=S, and Se) onto the surface of gold.
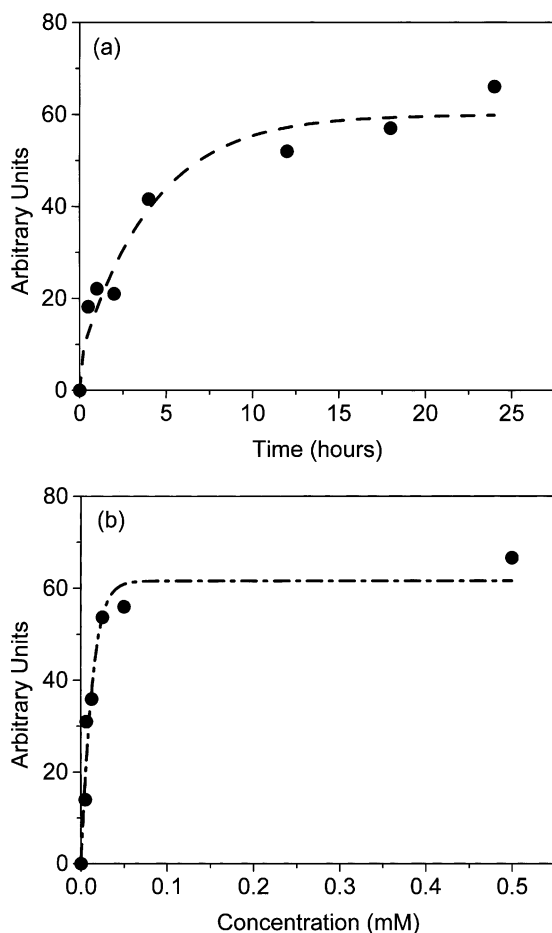
Fig. 3. Variation of film thickness from ellipsometric thickness after 24 h of deposition using $[Fe_3(CO)_9Se]^-$ concentrations ranging from 0.05 to 0.5 mM in methanol. (b) Ellipsometric thickness as a function of time (1–24 h) using $[Fe_3(CO)_9Se]^-$ at a concentration of 0.5 mM in methanol.

thickness of organic (and thus organometallic) thin films obtained from ellipsometric measurements is often unreliable (due to anisotropy and/or errors associated with the use of an appropriate refractive index), ellipsometric data nevertheless provide a useful probe of *relative* thickness for a series of structurally and compositionally similar films. Given these considerations, the data in Fig. 3a,b show that the thickness increases with both increasing concentration and time, but levels off with time. The data are consistent with a model of self-assembled film formation, showing a progressive growth until a plateau is reached, in which maximum growth has been achieved.

The quality of our Au substrates was checked by imaging hexagonal Au(111) lattices before depositing molecular films. Because of the soft nature of the molecular film and strong capillary interactions between molecules and normal AFM tips under ambient conditions, stable AFM imaging was only possible with dodecylamine-coated tips [17]. The topographic images

in Fig. 4 show the molecular films on typical Au(111) substrates comprised of atomically flat regions, as well as deep valleys. The molecular film on the atomically flat Au(111) area shows *z*-corrugation of ~ 2 nm. The normal force images provide clear contrast of the lateral structures on the molecular films. Well-ordered crystalline lattice structure of the molecular films was not observed from AFM measurements. Since AFM can show only surface structures, it is difficult to determine the exact film thickness via this technique.

Since it proved difficult to determine the thickness and the absolute surface coverage from the previous analyses, we attempted to examine the latter using QCM. Although this method does not reveal the exact thickness of the film (where different packing schemes are possible), it gives information on how much cluster material is present, and therefore a calculation of how many layers are formed is possible. The adsorption of $[HFe_3(CO)_9E]^-$ directly onto gold electrodes revealed plateaus in the mass changes at ~ 200 ng cm^{-2} within 2.5 min of deposition and at ~ 400 ng cm^{-2} within
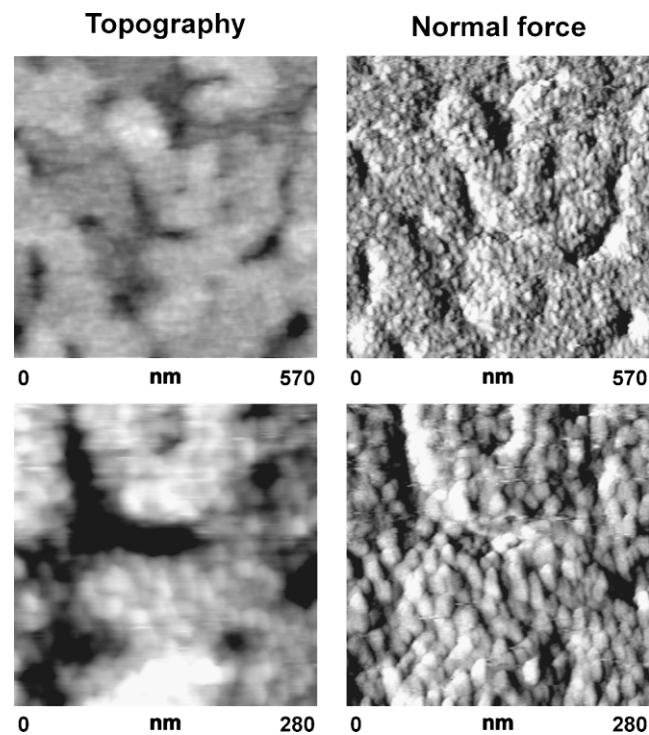

Fig. 4. Typical AFM topographic (constant force imaging) and normal force images (constant height imaging) of the molecular films taken from the same sample area. Topographic images are taken with a contact force ~ 1nN. The normal force images can be obtained by utilizing *slow* AFM feedback with a fixed contact force setting (1 nN) so that the AFM piezotube is not following the detailed structures on the surface, while still following the overall slope of the substrate. The topographic images show 2-nm corrugation on the molecular layers. The normal force images are presented here to show the lateral structures of the molecular films. Please note that both images are convoluted by the limited AFM tip diameter (~ 5 nm).
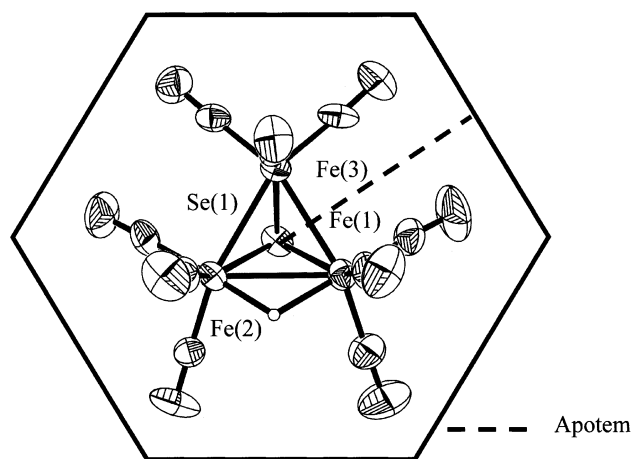
Fig. 5. Graphic representation of model used for the calculation of theoretical coverage in QCM experiments. The apothem value used considers van der Waals' forces. The estimated area per molecule is ~56 Å^2.

2.75 min of deposition. Surface coverages determined from the QCM measurements were 2.97×10^{-10} mol cm^{-2} (1.79×10^{14} molecules cm^{-2}) for the former plateau and 5.95×10^{-10} mol cm^{-2} (3.58×10^{14} molecules cm^{-2}) for the latter plateau, which compares well to the values predicted using a model based on crystallographic data [16,20], 2.99×10^{-10} mol cm^{-2} (1.79×10^{14} molecules cm^{-2}) for a monolayer and 5.98×10^{-10} mol cm^{-2} (3.58×10^{14} molecules cm^{-2}) for a bilayer. While the clusters have a diameter of approximately 8.5 Å, suggesting that a 41-Å film could have four layers, the presence of countercations with a similar diameter would account for a bilayer formation. Fig. 5 illustrates the model used for the calculation of the theoretical coverage. The presence of a second $[HFe_3(CO)_9Se]^-$ layer is also supported by the XPS data, since signals due to both bound and unbound cluster-selenium were present.

Fig. 6 shows representative XPS spectra of the bulk organometallic complex (deposited as a powder on a silicon wafer) and spectra of the corresponding self-assembled film on gold. The chemical composition of the organometallic cluster films determined by XPS on the elements Se 3d, Fe 2d, and C 1s supports the attachment of the cluster compounds to the surface of gold. When analyzing the XPS data for C 1s and Fe 2p, we found that the peaks in the bulk and the film were indistinguishable. In contrast, while we observed two peaks at 57 and 60 eV for Se 3d in the powder sample, we observed three peaks at 55, 57 and 60 eV for Se 3d in the self-assembled film. The two Se 3d peaks found in the powder correspond to cluster Se (57 eV), and oxidized Se (60 eV); we do not know the exact nature of the oxidized Se species. In the film, the presence of a dominant new Se 3d peak at 55 eV (i.e. a shift of 2

eV to lower energy than the unbound Se peak) is consistent with binding of the cluster to the gold through Se, given that a decrease from 164 to 162–163 eV is routinely observed for the S $2p_{3/2}$ peak when alkanethiols or disulfides bind to gold. The presence of three Se peaks in the film is consistent with a model in which
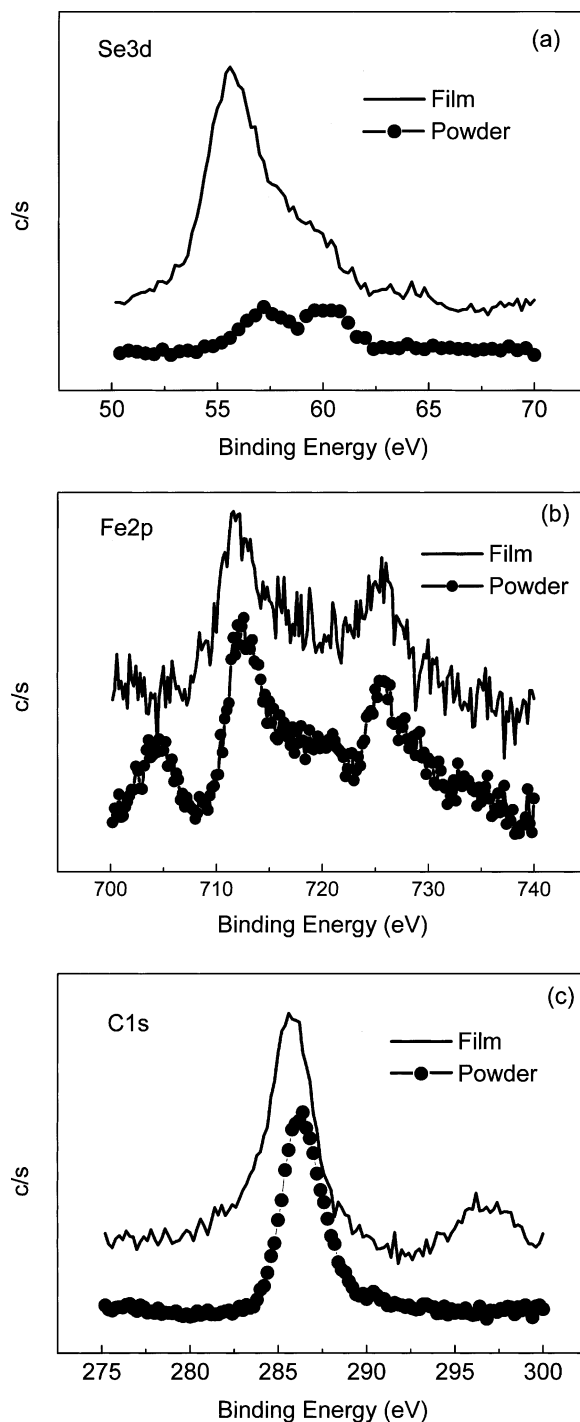

Fig. 6. Comparison of the XPS spectra of bulk $[Fe_3(CO)_9Se]^-$ vs. a self-assembled film of $[Fe_3(CO)_9Se]^-$ on Au for the elements (a) Se$_{3d}$ (b) Fe$_{2p}$ and (c) C$_{1s}$.

Table 1
XPS-derived distribution of selenium species upon exposure of $[HFe_3(CO)_9Se]^-/Au$ self-assembled films to air

Exposure time	Bound Se (%)	Free Se (%)	Free oxidized Se (%)	Total Se (%)
0	58	33	9	100
1 week	46	43	11	100

to air, the bound Se 3d decreases to 46%, while the unbound Se 3d increases to 43%, and the oxidized Se 3d increases to 11%. The stability of the films is remarkable, given that the parent cluster complexes decompose within a few hours upon exposure to air.

4. Conclusions

Chalcogen-bound cluster species were detectable by XPS and IR spectroscopy after adsorption of organometallic cluster molecules of the type $[Fe_3(CO)_9E]^{2-}$ and $[HFe_3(CO)_9E]^-$ (where E = S, Se and Te) onto the surfaces of gold. The binding of Se to gold was verified by the observation of a shift in the Se 3d XPS peak from 57 to 55 eV. The presence of two minor additional selenium species was also detectable by XPS, indicating the presence of an unbound cluster complex and a minor oxidized complex. Studies of the adsorption by QCM indicated the formation of a cluster monolayer, followed by the rapid formation of a second layer. The X-ray diffraction data are consistent with the presence of a bilayer rather than a monolayer structure.

Acknowledgements

The Robert A. Welch Foundation (grants C-0976, E-1207, and E-1320) and the National Science foundation (Grant CHE-9983352 to KHW and a CAREER Award CHE-9625003 to TRL) provided generous support for this research. This work made use of MRSEC Shared Experimental Facilities by the National Science Foundation under award number DMR-9632667.
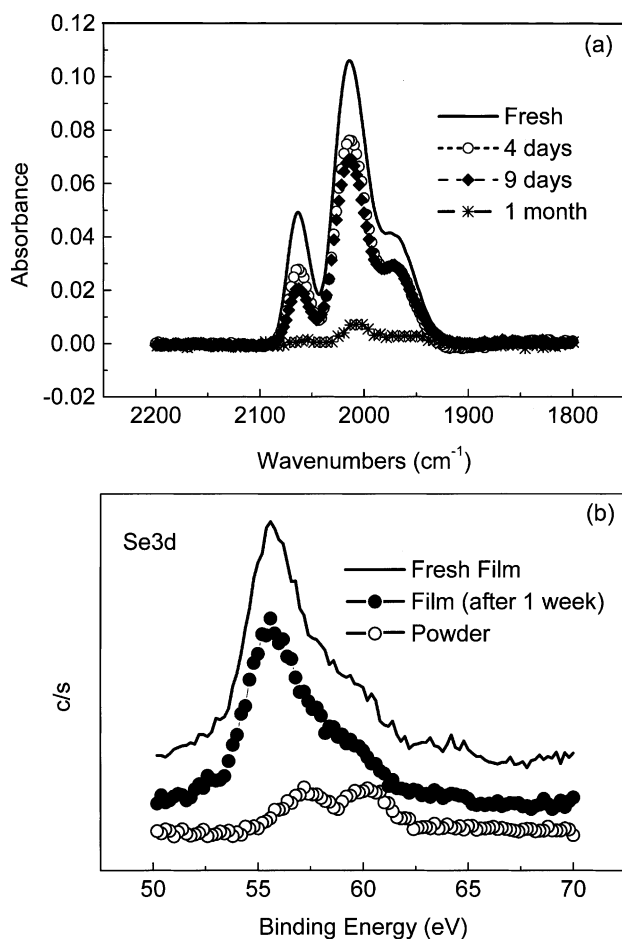
Fig. 7. (a) PM-IRRAS spectra of $[Fe_3(CO)_9Se]^-$ on Au after exposure to ambient environment at time = 0, 4 days, 9 days, and 1 month. (b) XPS spectra of $[HFe_3(CO)_9Se]^-$: bulk sample at time = 0 and on Au (Se$_{3d}$ region) after exposure to ambient environment at time = 0 and 1 week.

there are unbound cluster molecules, oxidized cluster molecules and a predominance of surface-bound cluster molecules.

The self-assembled cluster surfaces were exposed to ambient laboratory air, and then analyzed using both PM-IRRAS and XPS to evaluate the air stability of the films. Fig. 7a,b demonstrate that the films are remarkably stable for a period of 1 week. Analysis by PM-IRRAS shows that after 1 month, the ν(C–O) bands are still observed in the film, but their intensity has decreased. The XPS data obtained from these experiments are shown in Fig. 7b and summarized in Table 1. The self-assembled film was studied by XPS, both immediately and 1 week after preparation. Following exposure to air for 1 week, the XPS peak intensities were observed to decrease relative to those of the freshly prepared film (Fig. 7b). Table 1 shows that the three Se species in the freshly prepared film are present in the following ratios: 58% bound Se 3d, 33% unbound Se 3d, and 9% oxidized Se 3d. After 1 week of exposure

References

[1] A. Ulman, Chem. Rev. 96 (1996) 1533.
[2] G.E. Poirier, Chem. Rev. 97 (1997) 1117.
[3] C.D. Bain, S.D. Evans, Chem. Br. 31 (1995) 46.
[4] D.S. Everhart, Chemtech 29 (1999) 30.
[5] T. Nakamura, H. Kondoh, M. Matsumoto, H. Nozoye, Langmuir 12 (1996) 5977.
[6] T. Nakamura, H. Kondoh, M. Matsumoto, H. Nozoye, Surf. Sci. 402–404 (1998) 701.
[7] M.G. Samant, C.A. Brown, J.G. II Gordon, Langmuir 8 (1992) 1615.
[8] M.H. Dishner, J.C. Hemminger, F.J. Feher, Langmuir 13 (1997) 4788.
[9] K. Vijayamohanan, K. Bandyopadhyay, T. Pradeep, M. Venkataramanan, Langmuir 15 (1999) 5314.

[10] T. Nakamura, R. Kimura, F. Matsui, H. Kondoh, T. Ohta, H. Sakai, M. Abe, M. Matsumoto, Langmuir 16 (2000) 4213.

[11] M. Ge, B. Zhong, W.G. Klemperer, A. Gerwith, J. Am. Chem. Soc. 118 (1996) 5812.

[12] N. Prokopuk, D.F. Shriver, Chem. Mater. 10 (1998) 10.

[13] D.F. Shriver, M.A. Drezdon, The Manipulation of Air-Sensitive Compounds, Wiley, New York, 1986.

[14] R.L. Holliday, L.C. Roof, B. Hargis, D.M. Smith, P.T. Wood, W.T. Pennington, J.W. Kolis, Inorg. Chem. 34 (1995) 4392.

[15] R.E. Bachman, K.H. Whitmire, Inorg. Chem. 33 (1994) 2527–2533.

[16] R.E. Bachman, K.H. Whitmire, J. van Hal, Organometallics 14 (1995) 1792.

[17] R.D. Piner, S. Hong, C.A. Mirkin, Langmuir 15 (1999) 5457.

[18] G. Sauerbrey, Z. Phys. 155 (1959) 206.

[19] M. Shieh, T.-F. Tang, S.-M. Peng, G.-H. Lee, Inorg. Chem. 34 (1995) 2797.

[20] A.V. Virovets, S.N. Konchenko, N.V. Podberezskaya, Zh. Strukt. Khim. 40 (1999) 62.